Observations of Stratospheric Aerosol Using CPFM Polarized Limb Radiances

C. A. MCLINDEN*

Department of Physics and Astronomy, York University, Toronto, Ontario, Canada

J. C. MCCONNELL+

Department of Earth and Atmospheric Science, York University, Toronto, Ontario, Canada

C. T. MCELROY+ AND E. GRIFFIOEN

Environment Canada, Downsview, Ontario, Canada

(Manuscript received 6 August 1997, in final form 13 January 1998)

ABSTRACT

The authors have used CPFM (composition and photodissociative flux measurement) polarized limb radiance measurements combined with a vector radiative transfer model to estimate stratospheric aerosol number density, extinction coefficient profiles, and size distribution. The CPFM spectroradiometer is flown on board the NASA ER-2 high-altitude research aircraft. The vertical and horizontal polarization components of limb radiance, nadir radiance, and horizontal flux are measured in the wavelength range 300–770 nm from approximately 5°–10° above to 5°–10° below the local horizon. Results from two flights during April and May 1997 as part of the Photochemistry of Ozone Loss in the Arctic Region in Summer campaign are presented. Aerosol characteristics are determined by forcing the model radiances and polarization to match the measurements. Results indicate number densities at 20 km are roughly 5–6 cm^{-3} with an effective radius of 0.17–0.20 μm. Number, surface area, and volume densities compare favorably with two in situ particle counters also flown on the ER-2.

1. Introduction

It is generally recognized that stratospheric aerosol particles consist of a submicron sulfate haze concentrated between the tropopause and an altitude of roughly 30 km. These particles are known to play an influential role in climate and chemistry. In addition, they can interfere with the remote sensing of trace gases (Bhartia et al. 1993). Stratospheric sulfates are also known to possess large spatial and temporal variability, especially as one of the main sources is through the conversion of SO_2, injected into the stratosphere via volcanic eruptions. Thus, a thorough knowledge of their widespread distribution as well as their physical and optical properties is essential to a better quantitative understanding of heterogeneous chemistry processes, climate change, and their sources, sinks, and transport. It is also essential for the accurate calculation of stratospheric radiation and photolysis rates. Finally, specific to the ER-2 flights, it is important to have an accurate description of stratospheric aerosol for forward modeling necessary when retrieving trace gases such as NO_2 or BrO.

From 1993 to the present, a spectroradiometer has been flown on the NASA ER-2 high altitude research aircraft. This instrument, part of the Composition and Photodissociative Flux Measurement (CPFM), measures the horizontal and vertical polarization components of limb radiance along a 10-point scan from approximately 5°–8° above to 5°–8° below the local horizon in the wavelength range 300–770 nm (McElroy 1995; McElroy et al. 1995). The aircraft typically cruises at an altitude near 20 km. Also measured are the nadir radiance and the horizontal flux, which have been used to estimate surface albedo (McLinden et al. 1997). The absolute limb radiance uncertainties are estimated to be about 8% in the visible and 10% in the near-UV. Radiance and polarization have proven to be very useful in determining aerosol mass characteristics (Brogneiz et al. 1997; Herman et al. 1986). Aerosol retrievals are performed using measurements from the Photochem-

* Current affiliation: Department of Earth System Science, University of California, Irvine, Irvine, California.

+ Additional affiliation: Department of Physics and Astronomy, York University, Toronto, Ontario, Canada.

Corresponding author address: Dr. Chris McLinden, Dept. of Earth System Science, University of California, Irvine, Irvine, CA 92697-3100.
E-mail: cmclinden@halo.ps.uci.edu

istry of Ozone Loss in the Arctic Region in Summer (POLARIS) campaign.

The remainder of this study is organized as follows. First, a description of the vector radiative transfer model and the retrieval algorithm are given. Following this are results from two POLARIS flights, which include number density profiles and size distributions. Finally, discussion and conclusions are presented.

2. Radiative transfer model including polarization

The model used in this study solves the vector radiative transfer equation in a plane-parallel inhomogeneous atmosphere (McLinden 1998). All polarization information is contained in the Stokes vector, **I,** a four-element column matrix (often written as a row matrix for convenience), $\{I, Q, U, V\}$. The first element, I, represents the total radiance. The second, Q, is the radiance linearly polarized in the directions parallel and perpendicular to a reference plane. The CPFM spectroradiometer measures the parallel and perpendicular components of limb radiance, denoted $I_\parallel$ and $I_\perp$ respectively. The relationship between these and the Stokes vector elements are

$$I = I_\parallel + I_\perp \tag{1a}$$

$$Q = I_\parallel - I_\perp \tag{1b}$$

so that the fraction of light linearly polarized is given by

$$\mathrm{LP} = -\frac{I_\parallel - I_\perp}{I_\parallel + I_\perp} = -\frac{Q}{I}. \tag{2}$$

The vector radiative transfer equation is solved using the successive orders of scattering solution technique. In this method the Stokes vector elements are calculated for photons scattered once, twice, three times, etc., with the total of each Stokes vector element being the sum of overall scattering orders (e.g., Hansen and Travis 1974). In addition, the azimuthal dependence of the Stokes vector elements and phase matrix elements are expanded out in a Fourier series.

The atmosphere is the *U.S. Standard Atmosphere* at 70°N for spring and extends from 0 to 100 km. To improve modeling of the limb, spherical corrections have been implemented. Integration of the source vector is done using spherical shells and by taking it as varying linearly with optical depth through each shell. In addition, the direct solar beam is attenuated in a spherical atmosphere. The surface is assumed to be both Lambertian and depolarizing. All angular integration is performed using Gaussian quadrature. Rayleigh scattering cross sections are calculated from an empirical formula (Nicolet 1984) and the depolarization factor (due to the anisotropy of N_2 and O_2) is taken as 0.0279 (Young 1980). Aerosol phase matrix elements and cross sections are calculated numerically using a Mie scattering code. The model has been thoroughly tested against tabulated results of other polarized radiative transfer models (Garcia and Siewert 1989; Evans and Stephens 1991; Stammes et al. 1989). All comparisons were made for homogeneous Mie or Rayleigh plane-parallel atmospheres using a wide range of optical thicknesses and solar angles. In all cases differences were found to be $<0.1\%$ (McLinden 1998).

3. Aerosol retrieval algorithm

The quantities to be retrieved are the aerosol number density vertical profile and the aerosol size distribution, assumed to be independent of altitude. It is further assumed that the refractive index for a 0.75 H_2SO_4 + 0.25 H_2O aerosol composition is appropriate. Refractive indices for this composition have been measured at 300 K (Palmer and Williams 1975) and they are adjusted to stratospheric temperatures using the Lorentz–Lorenz relation (e.g., Steele and Hamill 1981). The size distribution is described in terms of an effective radius, r_{eff}, and an effective variance, v_{eff}. These are useful quantities as they take into account the fact that larger particles tend to be more efficient scatterers. The mathematical definitions for r_{eff} and v_{eff} are given in the appendix.

The ER-2 flights used were from 26 April 1997 and 6 May 1997, both out of Fairbanks, Alaska (65°N, 148°W). The two flight tracks are shown in Fig. 1. Results are presented from 2100 UTC (83°N, 148°W; SZA = 70°) 26 April 1997 and 2215 UTC (75°N, 108°W; SZA = 61°) 6 May 1997. All limb scans used were during clear-sky conditions. The surface is believed to be predominantly snow and ice-covered snow, which is modeled as a Lambertian reflector. The albedo was obtained using the nadir and horizontal flux fields, also measured by the CPFM, using the general method described in McLinden et al. (1997). Only limb scans in which the previous and subsequent scans had similar radiance and polarization values were selected. This is important as it takes about 15 min to complete a scan, during which time the aircraft has traveled about 150 km.

As the CPFM spectroradiometer measures radiance from 300 to 770 nm, there is a great deal of flexibility as to what wavelength(s) to use. As an initial constraint, all wavelengths at which significant gaseous absorption occurs were ruled out. This eliminates 300–330 nm and 480–680 nm due to absorption by ozone. Absorption by NO_2 occurs from 400 to 460 nm. There are also O_2 absorption bands centered near 760 nm. Therefore, three wavelengths are selected: 340, 475, and 750 nm. In general, longer wavelengths should be better suited because with a λ^{-4} dependence on Rayleigh scattering the fraction of the signal due to scattering by aerosols will be greater.

The retrieval algorithm can be roughly divided into two parts: 1) determining the extinction coefficient profiles using the limb radiances and 2) determining the

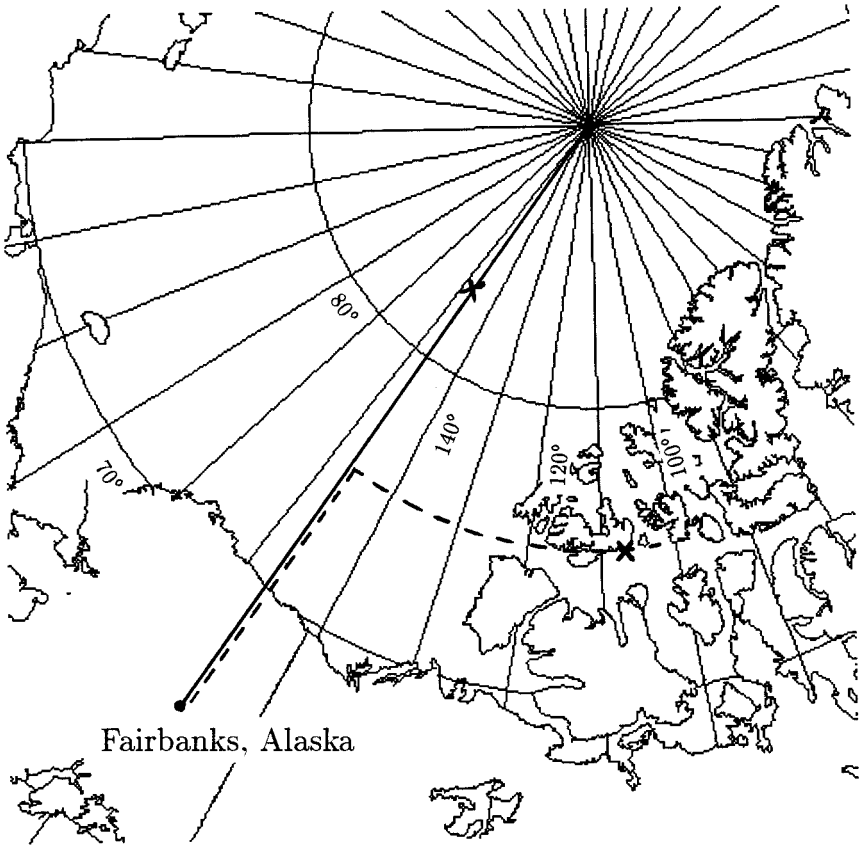

FIG. 1. Flight track for 26 April 1997 (solid) and 6 May 1997 (dashed), both north out of Fairbanks, Alaska. The ×'s denote the location at which the retrievals were carried out.

size distribution using the limb polarization and the previously determined extinction coefficient profile.

a. Extinction coefficient profiles

The limb radiances are sensitive mainly to the aerosol optical thickness along the line of sight and less so to the details of the size distribution as long as $\alpha \geq 1$, where $\alpha = 2\pi r_{\text{eff}}/\lambda$ is the aerosol size parameter and λ is wavelength. This is because the phase function (or the P_{11} element of the phase matrix) changes slowly with particle size. The exception is when the Rayleigh limit is approached, or roughly when $\alpha < 1$. For $r_{\text{eff}} = 0.2$ μm, a typical size for stratospheric sulfates, $\alpha = 1.7$ at 750 nm and $\alpha = 3.7$ at 340 nm. Thus, radiances at shorter wavelengths are quite insensitive to changes in aerosol size, assuming the optical thickness is constant. Changes in r_{eff} by $\pm 50\%$ resulted in a variation in radiance of $<1\%$ for a CPFM simulated limb scan. At 750 nm, varying r_{eff} by $+50\%$ resulted in a maximum change in limb radiance of $<1\%$ but varying it by -50% resulted in a maximum change of about 5%. Further calculations revealed that the phase function remains stable at 750 nm for $r_{\text{eff}} \geq 0.12$ μm. This radius is also representative of the lower limit of stratospheric sulfates (Kent et al. 1995), indicating that 750 nm should be useful in determining extinction profiles, irrespective of the size distribution.

On this basis, a constant lognormal size distribution (defined below) having equivalent size parameters of $r_{\text{eff}} = 0.2$ μm and $v_{\text{eff}} = 0.28$ is used in determining the extinction coefficient profile. In addition, only the limb radiances will be used, as polarization is sensitive to the details of the size distribution. For convenience, the extinction coefficient profile is assumed to be well represented by

$$\log k(\lambda, z) = a(\lambda) + b(\lambda)z + c(\lambda)z^2 + d(\lambda)z^3, \quad (3)$$

following the model of McCormick et al. (1996), where z is the altitude above the tropopause (km) and k is the aerosol extinction coefficient (km^{-1}). The extinction coefficient can be interpreted as the aerosol optical depth per unit (physical) length and is the product of number density and cross section. The advantage of using this approach is that the lower-midstratosphere extinction coefficient profile can be expressed using only four parameters. This is especially useful if the results are to be used in models. A drawback of this approach is that small-scale structure cannot be captured. As a result of the geometry, only limited aerosol profile information

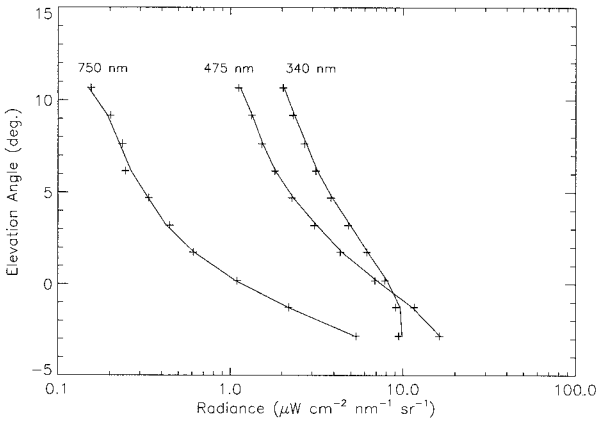

FIG. 2. CPFM radiances made at 2100 UTC 26 April 1997 (pluses) and model radiances (lines) based on minimized ϵ_o values of *a*, *b*, *c*, and *d* at 750 nm, 470 nm, and 340 nm.

can be extracted as there is an information overlap between uplooking scan steps. It was shown in a previous study that limb radiances were largely insensitive to the amount of aerosol below the lowest point along the line of sight and hence the tropospheric aerosol profile is less important (McLinden et al. 1998). The tropospheric aerosol extinction coefficient adopted is from upper-tropospheric Stratospheric Aerosol and Gas Experiment (SAGE) II measurements for background aerosol conditions (Kent et al. 1995).

The coefficients *a*, *b*, *c*, and *d* are determined by minimizing the difference of the measured and modeled limb radiances. The rms difference, ϵ_o, is the quantity to be minimized,

$$\epsilon_o = \sqrt{\frac{\sum_{i=1}^{M} [I_m^i - I^i(a, b, c, d)]^2}{M}}, \qquad (4)$$

where I_m^i represents the measured radiance at the *i*th step in the limb scan, $I^i(a, b, c, d)$ is the calculated radiance using (3), and M is the number of steps in the scan. Limb scan steps that probed below the tropopause were excluded. An estimate of the uncertainty can be obtained for each parameter by varying it until ϵ_o is 10% larger than the minimum, following the approach of Sato et al. (1996). The value of 10% was chosen as it represents the absolute uncertainty in the limb radiance. Model radiances were observed to be relatively insensitive to the value of *d* at all wavelengths. This suggests that much of the aerosol information is for altitudes below that at which the $d(\lambda)z^3$ term from (3) becomes important.

This procedure was carried out at 340, 475, and 750 nm. The limb radiances are shown as a function of elevation angle in Fig. 2 for the scan made at 2100 UTC 26 April 1997. Elevation angle is defined as the angle above (positive) or below (negative) the local horizon. For these scans, the height of the tropopause is estimated

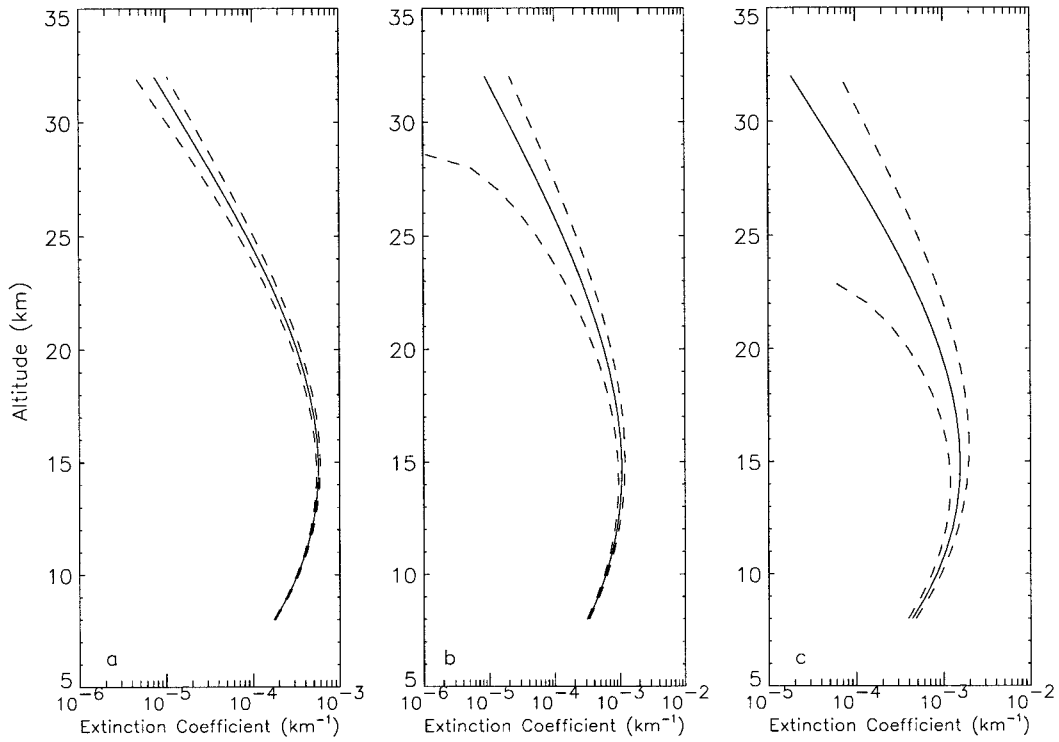

FIG. 3. Extinction coefficient profiles based on minimized ϵ_o values of *a*, *b*, *c*, and *d* at (a) 750 nm, (b) 475 nm, and (c) 340 nm for 2100 UTC 26 April 1997.

TABLE 1. Retrieved aerosol extinction coefficient profile parameters for eq. (3).

Date	Wavelength (nm)	a	b ($\times 10^{-1}$)	c ($\times 10^{-2}$)	d ($\times 10^{-4}$)
26 Apr 1997	340	-3.36 ± 0.10	1.70 ± 0.06	-1.45 ± 0.12	2.10 ± 0.24
	475	-3.49 ± 0.06	1.67 ± 0.04	-1.47 ± 0.07	2.09 ± 0.16
	750	-3.75 ± 0.02	1.60 ± 0.025	-1.40 ± 0.025	2.06 ± 0.15
6 May 1997	340	-3.15 ± 0.10	1.31 ± 0.06	-1.48 ± 0.12	2.31 ± 0.24
	475	-3.28 ± 0.06	1.28 ± 0.04	-1.50 ± 0.07	2.30 ± 0.16
	750	-3.50 ± 0.02	1.50 ± 0.025	-1.37 ± 0.03	2.17 ± 0.15

to be about 8 km. There is excellent agreement at all three wavelengths. The extinction coefficient profiles and the uncertainties are shown in Fig. 3 at the three wavelengths, while the extinction coefficient parameters are provided in Table 1. The extinction coefficient uncertainties are calculated based on the uncertainties in a, b, c, and d as follows:

$$\Delta k = k[(\Delta a) + (\Delta b)z + (\Delta c)z^2 + (\Delta d)z^3]. \quad (5)$$

Note that the uncertainties at 340 nm are quite large as the radiances are relatively insensitive to the aerosol due to increased multiple scattering and molecular scattering. At 20 km, aerosols account for roughly 20% of the total scattering. In contrast, the 750-nm radiance is quite sensitive to aerosol amount and vertical distribution as even slight changes in the aerosol profile induce substantial increases in ϵ_o.

b. Size distribution

It is convenient to employ an analytic expression to represent the size distribution so that the entire distribution can be described by a few parameters. Also, it has been shown that for all but recent posteruption periods, the majority of the aerosols are in a single mode. In this case, all major characteristics of a distribution can be obtained from two parameters, so the lognormal size distribution (Hansen and Travis 1974) is employed:

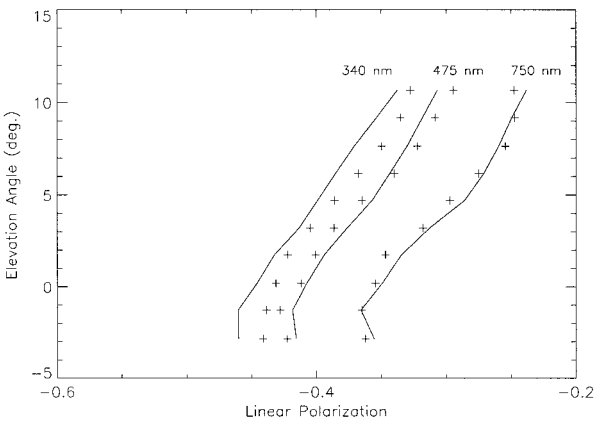

FIG. 4. CPFM polarization made at 2100 UTC 26 April 1997 (pluses) and model polarization (lines) based on minimized ϵ_o values of r_g and σ_g at 750 nm, 475 nm, and 340 nm.

$$n(r) = \frac{1}{\sqrt{2\pi}\,\sigma_g}\frac{1}{r}\exp\left[-\left(\frac{\ln r - \ln r_g}{\sqrt{2}\,\sigma_g}\right)^2\right], \quad (6)$$

where r_g and σ_g are size parameters and $n(r)$ is the size distribution defined such that $n(r)dr$ represents the number of particles with radii between r and $r + dr$. It is normalized such that $\int_0^\infty n(r)\,dr = 1$. It is assumed that the size distribution is height independent, or nearly so, so that one distribution is representative of the aerosol at all heights in the lower stratosphere. The parameters r_g and σ_g are related to the effective radius and variance via

$$r_{\text{eff}} = r_g e^{5\sigma_g^2/2} \quad (7a)$$

$$v_{\text{eff}} = e^{\sigma_g^2} - 1. \quad (7b)$$

Using the previously determined extinction coefficient profile, the size parameters can be determined in an analogous fashion using the limb polarization. Polarization is much more sensitive to the details of aerosol size distribution and hence is ideal for its retrieval. The rms difference is minimized to determine the size parameters r_g and σ_g,

$$\epsilon_o = \sqrt{\frac{\sum_{i=1}^{M}[\text{LP}_m^i - \text{LP}^i(r_g, \sigma_g)]^2}{M}}, \quad (8)$$

where LP_m^i is the measured polarization at the ith step in the scan and $\text{LP}^i(r_g, \sigma_g)$ is the model polarization. Uncertainty estimates in r_g and σ_g are determined by varying each until ϵ_o is 10% larger than the minimum. Hansen and Hovenier (1974) and Sato et al. (1996) used a similar approach to determine the size distribution and refractive index of sulfates in the Venusian atmosphere. The polarization scans at 340, 475, and 750 nm for 2100 UTC 26 April 1997 are shown in Fig. 4. In general, polarization is seen to decrease with increasing wavelength due to a decreasing contribution from Rayleigh scattering. The best agreement between model and measurement occurs at 750 nm and the worst agreement at 340 nm. Even at 750 nm there appears to be some fine structure that the model did not capture. This is likely due to the fact that the actual size distribution is height dependent and this retrieval process can only determine a single ''effective'' size distribution. The increasingly worse comparison at shorter wavelengths is due in part

TABLE 2. Retrieved size distribution parameters.

Date	r_g (μm)	σ_g	r_{eff} (μm)	v_{eff}
26 Apr 1997	0.12 ± 0.02	0.44 ± 0.04	0.20 ± 0.03	0.21 ± 0.03
6 May 1997	0.10 ± 0.02	0.46 ± 0.04	0.17 ± 0.03	0.24 ± 0.03

to error propagation in the extinction profile. Although the model agrees quite well with the 340-nm measured radiances, the estimated error is in the retrieved extinction coefficient profile is observed to be quite large. Again, this is due to the decreased relative contribution of aerosol scattering to total scattering.

The resultant size parameters from the 750-nm polarization are given in Table 2 and the size distributions are shown in Fig. 5 for each of the scans studied. Values for r_{eff} were found to be 0.20 ± 0.03 μm and 0.17 ± 0.03 μm for the scans from 26 April 1997 and 6 May 1997, respectively. Both are larger than the minimum 0.12 μm required for the extinction coefficient retrieval process to be insensitive to size distribution. Using 475-nm or 340-nm polarization to obtain size information resulted in estimated uncertainties in excess of ±0.08 μm. This, combined with the larger errors from the extinction coefficient profiles at these wavelengths, makes their use less than ideal.

c. Number density profile

The number density vertical profile $N(z)$ can be recovered from extinction coefficient profile using

$$N(z) = \frac{k(\lambda, z)}{\sigma_M(\lambda)}, \tag{9}$$

where σ_M is the Mie scattering cross section and can be calculated exactly for a given size distribution and refractive index. Using the 750-nm extinction and size distribution, the two number density profiles have been calculated and are shown in Fig. 6. There is maximum at 15 km of 10 cm^{-3} at 2100 UTC 26 April 1997 and a maximum at 12 km of 20 cm^{-3} at 2215 UTC 6 May 1997. Above this there was a steady decrease.

As an internal consistency check, the 20-km extinction coefficient was calculated using

$$k(\lambda, z) = \frac{\sigma_M(\lambda)}{\sigma_M(750\text{ nm})} k(750\text{ nm}, z) \tag{10}$$

and compared with the 20-km extinction coefficients at 340 and 475 nm as determined separately using the procedure outlined in section 3a. The agreement was found to be reasonable and within the estimated uncertainties indicating that size parameters are reasonable. At 30 km, the agreement was not quite as good, which is likely due to the fact that the actual aerosol size distribution is not truly independent of height.

d. Measurement intercomparison

1) IN SITU PARTICLES COUNTERS

Also flown on the ER-2 were two in situ aerosol counters. The first is the ER-2 Condensation Nucleus Counter II, which counts particles with radii between 0.004 and 1 μm (Wilson et al. 1983). The second is the Focused Cavity Aerosol Spectrometer (FCAS) II, which detects particles with radii between 0.004 and 1 μm (Jonsson et al. 1995). The FCAS II also measures aerosol surface area per unit volume and aerosol volume per unit volume. For comparison with retrieved aerosol densities at ER-2 height, the surface area and volume densities for the lognormal size distribution can be computed:

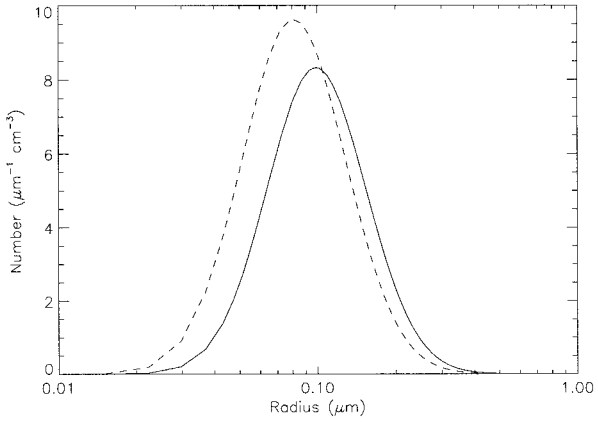

FIG. 5. Recovered size distributions based on minimized ϵ_o of r_g and σ_g for 2100 UTC 26 April 1997 (solid) and 2215 UTC 6 May 1997 (dashed).

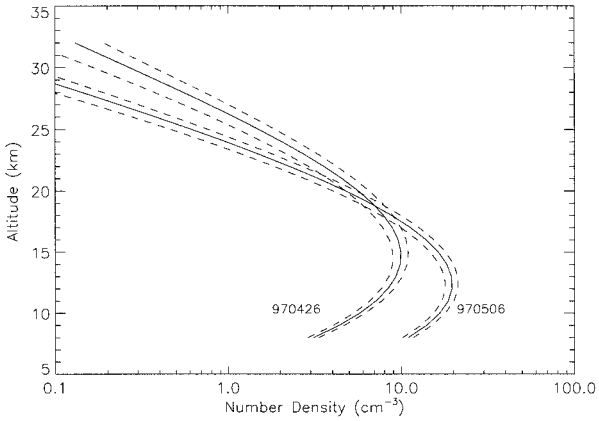

FIG. 6. Recovered number density profiles from 2100 UTC 26 April 1997 and 2215 UTC 6 May 1997.

TABLE 3. Comparison of retrieved aerosol properties with ER-2 particle counters.

	N (z_{ER2}) (cm^{-3})			S A (z_{ER2}) (μm^2 cm^{-3})		$V(z_{ER2})$, μm^3 cm^{-3}	
Date	CPFM	CNC-II*	FCAS-II*	CPFM	FCAS-II*	CPFM	FCAS-II*
26 Apr 1997	6.2 ± 0.9	4.9–9.3	4.1–5.5	1.7 ± 0.3	0.8–1.3	0.11 ± 0.027	0.038–0.14
6 May 1997	5.7 ± 0.9	4.4–5.5	3.9–4.8	1.1 ± 0.2	0.9–1.2	0.062 ± 0.016	0.056–0.090

$$\mathrm{SA}(z) = N(z)4\pi r_g^2 e^{2\sigma_g^2} = N(z)4\pi \frac{r_{\mathrm{eff}}^2}{(1+\upsilon_{\mathrm{eff}})^3} \quad (11a)$$

$$V(z) = N(z)\frac{4\pi}{3} r_g^3 e^{9\sigma_g^2/2} = N(z)\frac{4\pi}{3}\frac{r_{\mathrm{eff}}^3}{(1+\upsilon_{\mathrm{eff}})^3}, \quad (11b)$$

where SA(z) is the lognormal surface area density and $V(z)$ is the lognormal volume density. The number, surface area, and volume density comparisons are given in Table 3. The CPFM values were evaluated using the number density value at the ER-2 altitude. For the particle counters, the measured range over the duration of the limb scan is listed. Overall, the agreement is quite good as all CPFM-determined values, within their uncertainties, fall into the in situ measured ranges over a limb scan. The good agreement between surface area and volume densities indicates that the CPFM-derived effective radius and variance are realistic.

2) SAGE II

General comparisons are made against 1.02-μm extinction coefficient profiles SAGE II measurements from the 1989–90 period. It is reasonable to use this period for comparisons as it represents a period of stratospheric minimum after the eruptions of El Chichón and other smaller volcanos (Thomason et al. 1997a). Similarly, the effects of the 1991 Mount Pinatubo eruption have decayed enough to reasonably suggest that the present period is also one of stratospheric minimum.

The 1.02-μm extinction coefficient profiles are calculated using (10) and compared with least squares fits of 1989–90 SAGE II data to (3) (McCormick et al. 1996). This comparison is performed simply to confirm that the extinction coefficient order of magnitude and general shape of the profile is similar. From Fig. 7, it is clear that this is so. SAGE II data from 1989–90 also estimates the effective radius at 70°N and 20 km to be in the range 0.10–0.15 μm (Kent et al. 1995), which is generally consistent with the values of 0.2 ± 0.03 and 0.17 ± 0.03 μm from this study. Also, the CPFM surface areas listed in Table 3 are comparable to the late 1994–early 1995 SAGE II surface areas at 20 km and 70°N (Thomason et al. 1997b).

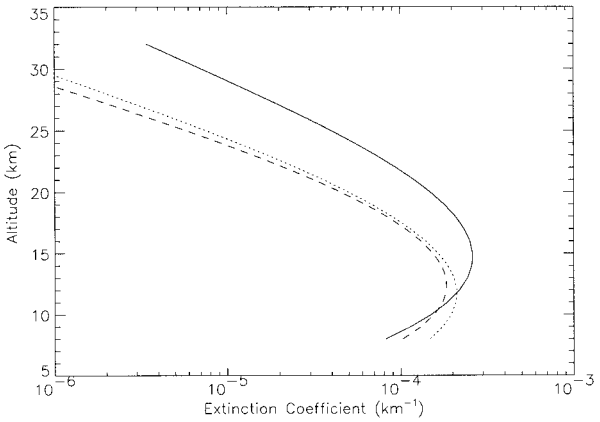

FIG. 7. Comparison of 1.02-μm extinction coefficients from 2100 UTC 26 April 1997 (solid), 2215 UTC 6 May 1997 (dashed), and SAGE II 1989–90 yearly average (dotted).

4. Conclusions

Stratospheric aerosol number density profiles, extinction coefficient profiles, and size distributions have been estimated using ER-2 CPFM polarized limb radiance measurements and a vector radiative transfer model. This was done using the radiances to determine the extinction coefficient profiles and the polarization to determine the size distribution. Results from a limb scan made at 2100 UTC 26 April 1997 indicate a maximum in number density at 15 km of 10 cm^{-3} with an effective radius of 0.20 μm and an effective variance of 0.21. Results from a limb scan made at 2215 UTC 6 May 1997 indicate a maximum in number density at 12 km of 20 cm^{-3} with an effective radius of 0.17 μm and an effective variance of 0.24. The increasing uncertainties of the extinction coefficient with increasing altitude combined with the relative insensitivity of the model radiances to the value of d suggest that these profiles may not necessarily be valid above approximately 30 km. The retrieved number, surface area, and volume densities at 20 km agree well with two in situ particle counters.

Improvements to this basic method should be possible using multiple wavelengths. Future studies will also be directed toward estimating how small errors in the CPFM viewing direction might impact aerosol retrievals. In addition, the feasibility of retrieving tropospheric aerosol information from the nadir radiance and polarization will be examined.

Acknowledgments. C. McL. would like to acknowledge the useful comments made by an anonymous reviewer. J. McC. wishes to thank the Natural Science and Engineering Research Council of Canada (NSERC) and the Atmospheric Environment Service (AES) for con-

tinuing support. C. McL. also wishes to thank J. Wilson for the use of his in situ measurements.

APPENDIX

Aerosol Size Parameters

The expression for the effective radius is

$$r_{\text{eff}} = \frac{\int_{r_1}^{r_2} r^2 n(r) r \, dr}{\int_{r_1}^{r_2} r^2 n(r) \, dr}, \tag{A1}$$

and that for the effective variance is

$$v_{\text{eff}} = \frac{\int_{r_1}^{r_2} (r - r_{\text{eff}})^2 r^2 n(r) r \, dr}{r_{\text{eff}}^2 \int_{r_1}^{r_2} r^2 n(r) \, dr}, \tag{A2}$$

where r_{eff}^2 in the denominator makes v_{eff} dimensionless (Hansen and Travis 1974).

REFERENCES

Bhartia, P. K., J. Herman, R. D. McPeters, and O. Torres, 1993: Effect of Mount Pinatubo aerosols on total ozone measurements from backscatter ultraviolet (BUV) experiments. *J. Geophys. Res.*, **98,** 18 547–18 554.

Brogniez, C., J. Lenoble, R. Ramananahérisoa, K. H. Fricke, E. P. Shettle, K. W. Hoppel, R. M. Bevilacqua, J. S. Hornstein, J. Lumpe, M. D. Fromm, and S. S. Krigman 1997: Second European Stratospheric Arctic and Midlatitude campaign: Correlative measurements of aerosol in the northern polar atmosphere. *J. Geophys. Res.*, **102,** 1489–1494.

Evans, K. F., and G. L. Stephens, 1991: A new polarized atmospheric radiative transfer model. *J. Quant. Spectrosc. Radiat. Transfer,* **46,** 413–423.

Garcia, R. D. M., and C. E. Siewert, 1989: The F_N method for radiative transfer models that include polarization effects. *J. Quant. Spectrosc. Radiat. Transfer,* **41,** 117–145.

Hansen, J. E., and J. W. Hovenier, 1974: Interpretation of the polarization of Venus. *J. Atmos. Sci.,* **31,** 1137–1160.

——, and L. D. Travis, 1974: Light scattering in planetary atmosphere. *Space Sci. Rev.,* **16,** 527–610.

Herman, M., J. Y. Balois, L. Gonzalez, P. Lecomte, J. Lenoble, R. Santer, and C. Verwaerde, 1986: Stratospheric aerosol observations from a balloon-borne polarimetric experiment. *Appl. Opt.*, **25,** 3573–3584.

Jonsson, H. H., J. C. Wilson, C. A. Brock, R. G. Knollenberg, R. Newton, J. E. Dye, D. Baumgartner, S. Borrmann, G. V. Ferry, R. Pueschel, D. C. Woods, and M. C. Pitts, 1995: Performance of a focused cavity aerosol spectrometer for measurements in the stratosphere of particle size in the 0.06–2.0-μm diameter range. *J. Atmos. Oceanic Technol.,* **12,** 115–129.

Kent, G. S., P.-H. Wang, M. P. McCormick, and K. M. Skeens, 1995: Multiyear Stratospheric Aerosols and Gas Experiment II measurements of upper troposphere aerosol characteristics. *J. Geophys. Res.,* **100,** 13 875–13 899.

McCormick, M. P., P. H. Wang, and M. C. Pitts, 1996: Background stratospheric aerosols and polar stratospheric cloud reference models. *Adv. Space Res.,* **18,** 155–177.

McElroy, C. T., 1995: A spectroradiometer for the measurement of direct and scattered solar irradiance on-board the NASA ER-2 high altitude research aircraft. *Geophys. Res. Lett.,* **22,** 1361–1364.

——, C. Midwinter, D. V. Barton, and R. B. Hall, 1995: Comparison of J-values estimated by the Composition and Photodissociative Flux Measurement with model calculations. *Geophys. Res. Lett.*, **22,** 1365–1368.

McLinden, C. A., 1998: Observation of atmospheric composition from NASA ER-2 spectroradiometer measurements. Ph.D. thesis, York University, 292 pp.

——, J. C. McConnell, E. Griffioen, C. T. McElroy, and L. Pfister, 1997: Estimating the wavelength-dependent ocean albedo under clear-sky conditions using NASA ER 2 spectroradiometer measurements. *J. Geophys. Res.*, **102,** 18 801–18 811.

——, ——, C. T. McElroy, and E. Griffioen, 1998: Sensitivity of polarized limb radiances to stratospheric aerosols with application to NASA ER-2 spectroradiometer measurements. *Atmospheric Ozone, Proc. Quadrennial Ozone Symp.,* R. D. Bojkov and G. Visconti, Eds., International Ozone Commission, 947–950.

Nicolet, M., 1984: On the molecular scattering in the terrestrial atmosphere: An empirical formula for its calculation in the homosphere. *Planet. Space Sci.,* **32,** 1467–1468.

Palmer, K. F., and D. Williams, 1975: Optical constants of sulphuric acid: Application to the clouds on Venus? *Appl. Opt.,* **14,** 208–209.

Sato, M., L. D. Travis, and K. Kawabata, 1996: Photopolarimetry analysis of the Venus atmosphere in the polar region. *Icarus,* **124,** 569–585.

Stammes, P., J. F. de Haan, and J. W. Hovenier, 1989: The polarized internal radiation field of a planetary atmosphere. *Astron. Astrophys.,* **225,** 239–259.

Steele, H. M., and P. Hamill, 1981: Effects of temperature and humidity on the growth and optical properties of sulphuric acid-water droplets in the stratosphere. *J. Aerosol Sci.,* **12,** 517–528.

Thomason, L. W., G. S. Kent, C. R. Trepte, and L. R. Poole, 1997a: A comparison of the stratospheric aerosol background periods of 1979 and 1989–1991. *J. Geophys. Res.,* **102,** 3611–3616.

——, L. R. Poole, and T. Deshler, 1997b: A global climatology of stratospheric aerosol surface area density deduced from Stratospheric Aerosol and Gas Experiment II measurements: 1984–1994. *J. Geophys. Res.,* **102,** 8967–8976.

Wilson, J. C., E. D. Blackshear, and J. H. Hyun, 1983: The function and response of an improved stratospheric condensation nucleus counter. *J. Geophys. Res.,* **88,** 6781–6785.

Young, A. T., 1980: Revised depolarization corrections for atmospheric extinction. *Appl. Opt.,* **19,** 3427–3428.